Self-Assembly and Applications of Ultraconcentrated Nanoparticle Solutions

Vladimir A. Turek, Laura N. Elliott, Arwen I. I. Tyler, Angela Demetriadou, Jack Paget, Michael P. Cecchini, Anthony R. Kucernak, Alexei A. Kornyshev, and Joshua B. Edel*

Department of Chemistry, Imperial College London, South Kensington Campus, London, SW7 2AZ United Kingdon

ABSTRACT We demonstrate a highly efficient method for concentrating, purifying and separating gold nanoparticles. The method relies on localized density gradients that can be formed at an aqueous | organic phase interface. We show that this method is able to concentrate aqueous gold nanoparticles to the point where confinement leads to variable interparticle separations. Furthermore, the physical properties of the resulting solution are drastically altered when compared to water. For example, densities higher than 4.5 g/cm^3 could be generated without nanoparticle aggregation. As far as we are aware, this is one of the highest reported densities of an aqueous solution at room temperature. Finally, the compositions of the solutions generated are highly dependent on parameters such as particle size and background analyte making this technique highly advantageous for the separation of multimodal NP populations and chemical purification, with 99.5% and >99.9% efficiency, respectively.

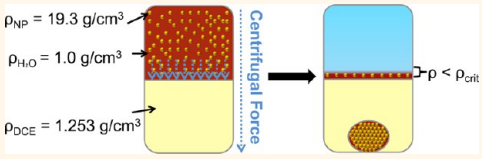

KEYWORDS: liquid−liquid interface · centrifugation · nanoparticles · purification · size separation · plasmon ruler

Nanoparticles (NPs) hold great promise in a vast number of fields including sensing,[1−3] catalysis,[4] medicine,[5,6] water treatment,[7] electronics,[8] solar cells[9] and optics.[10] Most of these applications require precise control over the NPs themselves in terms of size, shape, concentration, monodispersity and the medium in which they are suspended. Furthermore, there has been intense research focused on the synthesis of ever more complex particles with unique properties,[11] such as complex nonspherical geometries,[12] or even NPs with unique surface chemistries.[13] However, some of the common chemicals used in these processes such as surfactants,[14] dyes,[15] and polymers[16] are difficult to remove completely and can be detrimental in some applications. The synthesis of nonspherical NPs generally also suffer from broad size and/or geometry distributions.[17] Finally, the NP concentration is an overlooked physical property of NP solutions. So called 'nanofluids' (colloidal solutions with a high nanoparticle content) display remarkably varied physical properties as a function of NP concentration; however, very few techniques exist that can efficiently increase the concentration without inducing irreversible aggregation.[18] There is therefore a need for efficient methods that will achieve size/shape separation and purify the NPs from chemical contaminants, as well as increase the concentration of NPs without aggregation. Here, we present a method which allows for the rapid formation of ultraconcentrated gold NP aqueous solutions. As far as we are aware, this is the highest density aqueous NP solution known to date. We also show that this method can lead to highly efficient chemical purification and size separation of NPs.

The general operating mechanism is as follows: In the presence of a denser organic phase, aqueous NPs can be driven to the liquid−liquid interface (LLI), or in our case aqueous|1,2-dichloroethane interface, by a centrifugal force. Provided that the difference in solvation energies[19,20] are high enough to prevent a transfer of NPs across the interface, this leads to an increase in the concentration of particles directly adjacent to the interface.The concentration gradient also gives rise to a density gradient which upon reaching a critical density, may induce instabilities at the interface, leading to the

* Address correspondence to joshua.edel@imperial.ac.uk.

Received for review June 20, 2013 and accepted September 26, 2013.

Published online September 26, 2013
10.1021/nn403131e

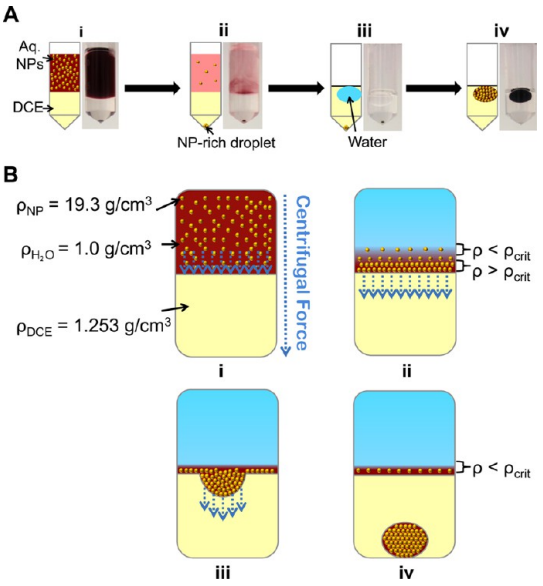

Figure 1. Schematic and mechanism of ultraconcentration. (A) Centrifugation of an aqueous nanoparticle solution in the presence of DCE (i) leads to an extremely concentrated NP droplet being formed at the bottom of the DCE (ii). The supernatant can be easily removed and replaced with pure water (iii), if contact is made with this phase the droplet can be redispersed (iv). (B) The centrifugal force acts on the NPs (i) and drives them to the interface (ii) above a critical threshold density, the interface is deformed (iii) and eventually a NP-rich droplet breaks off from the main aqueous phase (iv).

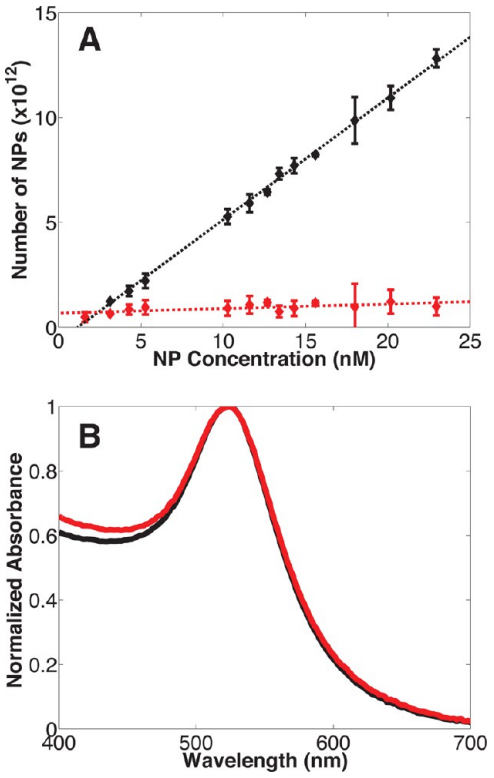

Figure 2. Characterization of the initial NP concentration dependence on the NP-rich droplet formation and the stability of the ultraconcentrated NPs. (A) Initial NP concentration dependence on the number of NPs in the droplet (black) and residual particles in the supernatant (red) at an initial NaCl equivalent concentration of 2.5 mM, centrifuged at 20 238*g* for 15 min. The constant residual NPs in the supernatant represents a threshold, below which no droplet is formed, while the NPs in the droplet follow a $y = 0.58x - 0.68$ dependency. (B) Comparison of the normalized absorbance of as made NPs (red) and a 20 000-fold dilution of the NP-rich droplet (black). The fact that no red-shifted 'shoulder' is seen in the spectrum of the diluted sample suggests that the method does not induce aggregation.

formation of NP rich droplets which sediment and merge at the bottom of the centrifuge tube (Figure 1A). It should be noted that droplet generation ensures that the particles remain dispersed in an aqueous environment, in other words, phase transfer does not occur. The critical density for this process is related to the following: the difference in density between the organic and aqueous phase, and the interfacial tension (a water|1,2-dichloroethane (DCE) interface has an interfacial tension of 28.1 mN/m at 20 °C; the DCE has a density of 1.253 g/cm^3 at 20 °C). The NP concentration in these droplets is high enough that electrostatic repulsion, screened by the ions of electrolyte, may induce local, short-range order. The interparticle spacing can be further controlled through the concentration of electrolyte, the increase of which will decrease the screening length. The resulting NP concentration levels at appropriate ionic strengths can exceed 3.7 g of Au/mL of solution, reaching densities of 4.5 g/cm^3

RESULTS AND DISCUSSION

Nanoparticle-Rich Droplet Formation and Concentration. Recently Turek *et al.* have demonstrated that centrifugation can be used to facilitate NP adsorption at a LLI made up of an aqueous solution consisting of NaCl and 16 ± 2.4 nm Au NPs functionalized with 12-mercaptododecanoic acid (MDDA) and DCE.[10] The particles adsorbed at the interface were characterized as a function of the ionic strength of the solution, relative centrifugal force, centrifugation time, pH, and the interfacial area. We build on this by operating with low ionic strength aqueous solutions (NaCl equivalent concentration of 1.0−8.5 mM) to limit NP adsorption and facilitate a concentration gradient at the LLI. By doing so, an aqueous droplet containing an extremely high NP concentration can be formed at the bottom of the DCE layer. Experimentally this was performed in a 2 mL centrifuge tube, consisting of 0.5 mL of DCE and 1 mL of NP solution, with a total number of NPs between 9.4×10^{11} and 1.4×10^{13}. To determine how many NPs transfer from the bulk to the droplet, the initial NP concentration in the bulk aqueous phase was varied between 1.5 and 23 nM (Figure 2B). A seemingly linear relationship was observed for the number of particles confined to the droplet with increasing initial concentration in the bulk of the aqueous phase; the percentage of the initial NPs confined to the droplet increased from 50% at 1.5 nM

to 93% at 23 nM as determined through UV−Vis spectroscopy. However, the number of residual particles in the supernatant remained approximately constant, at a value of $\approx 9.4 \times 10^{11}$ NPs irrespective of the initial concentration. This constant value is a threshold for the minimum number of NPs needed for this method to work—below this, no droplet is formed. On the basis of these observations, the mechanism that is proposed for the droplet generation is shown in Figure 1B. Upon centrifugation the NPs in the aqueous phase are driven to the interface (Figure 1B i), if the initial number of particles is above the threshold value, then the local density of the aqueous side of the interface is increased (Figure 1B ii) to the point where it is energetically more favorable to generate "extra" interfacial area (Figure 1B iii). Once the density gradient is established, the droplets break away from the interface and sediment at the bottom of the DCE phase (Figure 1B iv). At this point, the residual particles in the supernatant are insufficiently concentrated to obtain a sufficient density gradient for this process to be repeated.

Since the formed droplet is an extremely concentrated gold NP solution, we need to significantly dilute the sample to recover the absorbance. The droplet, formed from an aqueous solution containing an equivalent of 1 mM NaCl (as assessed from conductivity measurements), revealed the absorbance at 525 nm to be 20 300 ± 19%. When an extinction coefficient of $4.916 \times 10^8 M^{-1}\ cm^{-1}$ was used,[21] the NP concentration in the droplet was determined to be $\approx 41.3\ \mu M$ or $2.49 \times 10^{16} \pm 4.70 \times 10^{15}$ NPs/mL. Given a weight per nanoparticle of $4.40 \times 10^{-17} \pm 1.94 \times 10^{-17}$ g, the total gold content of this solution is 1.10 ± 0.53 g Au/mL. Interestingly, the density of this solution was determined to be 2.24 ± 0.64 g/cm^3 (*cf.* Supporting Information). It should be noted that the density and dilution values are in agreement on the estimated NP concentrations, *i.e.*, from the density (assuming a negligible density contribution from the ions and NP functionality) the weight of gold in the solution would be 1.30 ± 0.67 g/mL.

It was decided to test whether the salt concentration can control the concentration of NPs by altering the screening length. It then follows that an increase of the ionic strength leads to higher NP concentrations. This was verified by monitoring the density of the resulting solution as a function of the ionic strength of the initial preconcentrated solution (1.0−8.5 mM equivalent NaCl). As shown in Figure 3A, a strong effect of NaCl content on the concentration of NPs in the droplet is observed. Surprisingly, at an initial NaCl concentration of 8.5 mM, the resulting NP-rich droplet has a density of 4.57 ± 0.26 g/cm^3 and is therefore higher than even a saturated Clerici solution at room temperature.[22] This density corresponds to a solution which is composed of almost 20 vol % gold. To the best of the authors' knowledge, this is the highest density aqueous solution that has been demonstrated at room temperature; however, it should be stressed that higher densities still are likely to be accessible with this method. Furthermore, the NP concentration of this solution is 9.09×10^{16} NPs/mL or 3.76 g of gold/mL; the optical density at 525 nm is therefore expected to

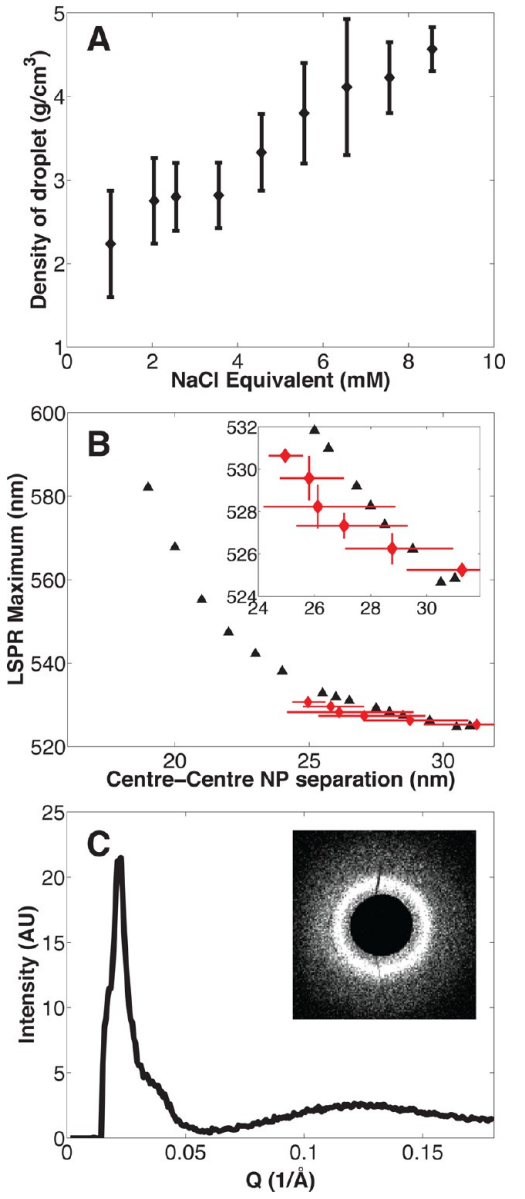

Figure 3. Tunable properties of the NP-rich droplet as a function of salt concentration. (A) Density of the resulting NP-rich droplet as a function of the ionic strength. There is a strong dependence between the density of the resulting droplet on the NaCl concentration, due to more efficient screening of the NPs' charge, reaching a density of 4.57 ± 0.26 g/cm^3 at an NaCl equivalent of 8.5 mM. (B) Experimental results (red) and simulations (black) of the LSPR maximum of the NP-rich droplet as function of the interparticle separations agree well with each other (note: experimental separations are approximated from the density). This indicates that the position of the NPs with respect to each other can be tuned by the ionic strength. (C) Low angle X-ray diffraction pattern of a solution made at 4.5 mM equivalent NaCl confirms there is positional correlation between the NPs, with a center−center separation of 29 nm.

be in excess of 74 000. Taking the surface of the MDDA as the edge of the physical radius of NPs (and assuming this functionality to provide a 1.5 nm steric coating), then this colloidal solution has an active surface area of 73 m^2/mL.

The strong dependence of the density on the NaCl concentration suggests that the separation between the particles is dictated by the ionic screening. If metallic NPs get close enough to each other, the coupling of localized plasmons in each of them leads to a red shift of the localized surface plasmon resonance (LSPR). Transmission measurements (see Supporting Information) of the resulting solutions (Figure 3B) made between 2.0 and 8.5 mM equivalent NaCl confirms that a red-shift between 525.2 ± 0.3 and 530.6 ± 0.2 nm is observed as the NaCl concentration is increased. From the densities of the solutions at these NaCl concentrations, the interparticle separations were estimated by assuming the particles reside as far away from each other as possible and a negligible contribution from the counterions and functionality to the overall density of the solution. A comparison of spectra obtained from Finite Integration Techniques (FIT) computer simulations (see Supporting Information) suggests that these LSPR maxima correspond to gold surface/gold surface separations between neighboring NPs of 10−15 nm.

These figures are supported further by X-ray diffraction (Figure 3C). A NP-rich droplet made at 4.5 mM NaCl equivalent shows a sharp interference peak in the small angle region which was interpreted as the first order peak of the particle−particle structure factor. This peak indicates that the average center−center interparticle separation is ≈29 nm. Working back from the density, the estimated center−center separation for this sample is 28.5 nm, which is in excellent agreement. Further experimentation is needed to fully characterize this, but there is strong evidence that this method is capable of concentrating NPs to levels at which the interparticle separations are controlled in 3 dimensions. The lack of long-range order in these samples is attributed to a relaxation of the compressive force when centrifugation is stopped; nevertheless the physical confinement and electrostatic repulsion give rise to short-range order.

Surprisingly, despite such high concentrations, there is no evidence of aggregation. Figure 2B shows a comparison between the normalized spectra of 'as-made' NPs and a 20 000-fold diluted sample from a NP-rich droplet made at 1 mM NaCl. Given even mild aggregation, the broadness of the dipole peak should increase; however, this is not observed in the diluted NPs' absorbance spectra. The lack of aggregation is likely due to the exceptional stability of MDDA stabilized NPs as described elsewhere.[10] Perhaps more surprising is that even citrate stabilized particles can be concentrated in this manner without initial

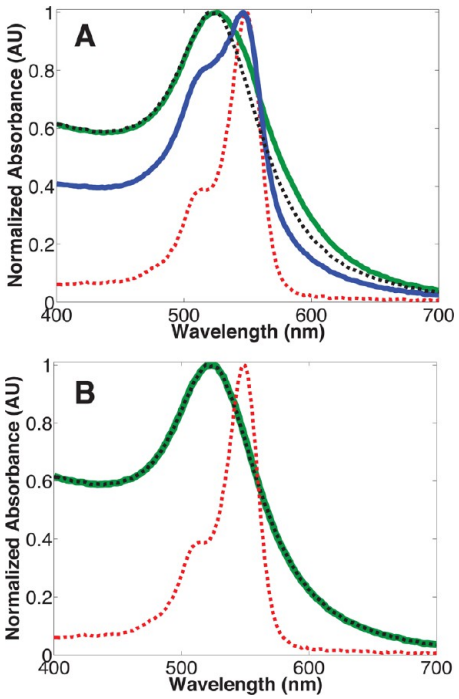

Figure 4. Comparison between conventional centrifugation and this method for the purification of NPs in the presence of a dye. (A) After a single step, conventional centrifugation (blue) is able to purify 95.2 ± 0.8% of the dye Rose Bengal (red dotted), while the second step (green) purifies an additional 90.0 ± 3.0% of the dye to a final purity of 99.5 ± 0.1%; when compared to as-made particles (black dotted), a clear shift in the absorbance spectrum can still be seen. (B) After a single step forming the NP-rich droplet, and redispersing in water (green) in excess of 99.9% of the dye is removed. So much so, that there is a negligible difference in the absorbance spectrum between the as-made and purified NPs. For both comparisons, the NP solutions were contaminated with 2 mM Rose Bengal and centrifugation was carried out at 20 238*g* for 15 min.

aggregation. However, it should be noted that citrate stabilized NPs have a short-lived stability and aggregate irreversibly within approximately 30 min of droplet formation. Despite this, it is hypothesized that the initial stability of citrate particles at these concentrations is due to the fact that the forces acting on the NPs with this method are the same as during conventional centrifugation. Consequently if the NPs do not aggregate during conventional centrifugation, the probability that the NPs will be stable in the high density droplet is greater; however, this stability may be short-lived. Naturally, the versatility of this method can be extended to systems other than Au NPs as long as the NPs to have a sufficiently high sedimentation coefficient.

An interesting question related to this is why the functionalized NPs are in principle able to come at such close surface-to-surface separations in electrolytic solutions while not fusing? This could be understood using the Donnan equilibrium, which potentially manifests itself here due to a spontaneous increase salt concentration as the NPs are pushed into close proximity.

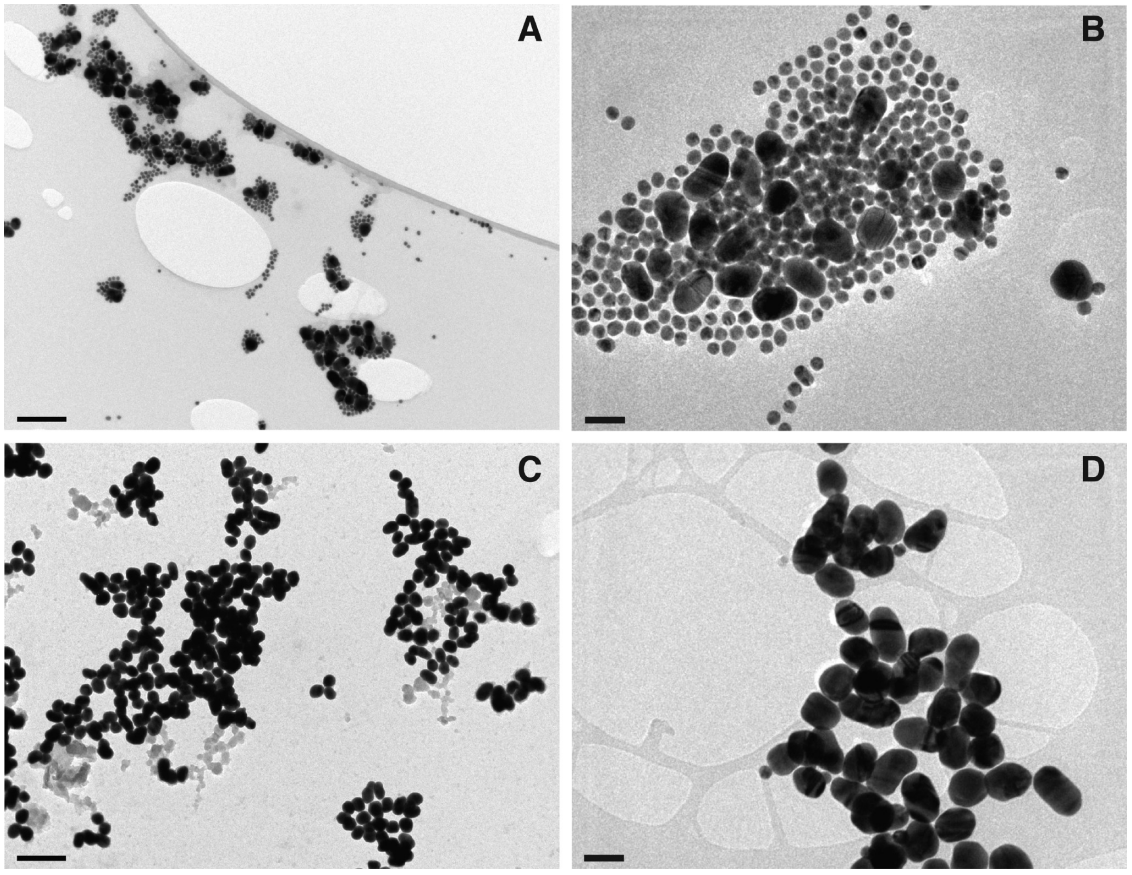

Figure 5. Demonstration of size separation of NP solutions. (A and B) Mixture of 16 and 43 nm gold particles. (C and D) Separated 43 nm particles after 15 min at 1503*g*. On the basis of the analysis of over 5000 NPs, there is a 99.5% removal of 16 nm NPs and a 210-fold enrichment of 43 nm particles. Scale bar for (A) and (C) is 200 nm, for (B) and (D) it is 50 nm.

Nanoparticle Purification and Size Separation. Dilution of the concentrated droplet back to as-made concentrations with DI water effectively acts as a purification mechanism. The LLI confines the particles to the droplet, which together with the high density of this solution makes its separation from the supernatant trivial. To test the levels of purification that can be achieved, a dye (Rose Bengal) was added to the aqueous NP solution (with a total of 8.9×10^{12} NPs) at a concentration of 2 mM. Conventional centrifugation was compared to the droplet generation method, as is shown in Figure 4. After a single step, conventional centrifugation removed $95.2 \pm 0.8\%$ of the dye, while the second step removed a further $90.0 \pm 3.0\%$, to give a total purity of $99.5 \pm 0.1\%$ after 2 steps. Conversely, a single purification step with our method leads to purity levels that could not be accurately measured by UV−visible spectroscopy (due to an almost perfect overlap between the purified and uncontaminated NPs), but is in excess of 99.9%. This purification can also be applied to reducing the ionic strength of the NP solution. For example, the conductivity of the initial NP solution was 217 μS/cm while diluting the droplet with ultrapure water back to the as-made concentrations leads to a reduced conductivity of 1.4 μS/cm. Reducing the ionic strength aids stabilization of the nanoparticles through the increase in Debye screening length.

The efficiency of the purification relies on a difference in the sedimentation coefficient of the particles and dissolved species. Because of a large difference between the size of the nanoparticles and chemical species, this process proves to be extremely efficient. However, the same principle can be applied to separate NPs of differing sizes. For example, Figure 5A shows a mixture of 16 nm MDDA and 43 nm citrate gold particles, mixed in a 1:1 (v/v) ratio of as-made solutions; this equates to approximately 6.0×10^{11} 16 nm and 3.1×10^{10} 43 nm NPs per mL. Centrifuging the mixture at 1503*g* for 15 min results in the formation of a droplet consisting predominately of 43 nm NPs, Figure 5B. It is worth noting that optimizing the RCF may maximize the separation efficiency; however, this was not investigated in detail. Analysis of electron microscopy images of over 5000 particles (done by manually counting the particles from SEM) showed that the ratio of 16:40 nm particles was 21.57 for the initial mixed solution, and 0.10 in the separated NP-rich droplet. This suggests a ≈210 enrichment of the 43 nm NPs. This has important implications in NP synthesis where multimodal size distributions are present. This is a common problem with more advanced NP

syntheses, where despite numerous reports in the literature describing nanometer control over the dimensions of nanoparticles, secondary nanostructures also arise. As an example, the "standard" gold nanorod synthesis[14] has exquisite control over the aspect ratio of the rods,[23] however 3 distinct particle populations are present – rods as well as large and small spheres.[24] Because of the properties of NPs being extremely size and shape specific,[25] these secondary particle contaminants are extremely deleterious to many of the applications that NPs promise. Indeed, one of the most time-consuming elements of many nonspherical nanoparticle syntheses is purification and size separation of the desired product. Naturally, the droplet formation process demonstrated here is a nonuniversal separation technique as only the larger particles (or those with a higher sedimentation coefficient) may be confined to the droplet. Furthermore, as Figure 2A demonstrated, a constant number of particles need to act as the 'sacrificial' particles for the critical density for droplet formation to be reached. If the smaller particles act as these sacrificial particles, then the separation efficiency is likely to be optimum, however if the concentration of the smaller particles becomes large enough to also form a droplet, then separation efficiencies are expected to be reduced. Nevertheless, if the conditions for separation are appropriately chosen, then this technique can be remarkably efficient for size separation. The speed, simplicity and efficiency that this technique offers are therefore highly pertinent to researchers working with NPs.

CONCLUSIONS

In conclusion, it has been demonstrated that by centrifuging a NP solution in the presence of a denser, insoluble phase (in this case water and DCE) after a single step, gold NP concentrations in excess of 3.7 g of gold/mL can be rapidly achieved. The density of the resulting aqueous phase can be tuned by the ionic strength and can exceed even the Clerici solution. At 8.5 mM NaCl equivalent, the density was determined to be 4.57 ± 0.26 g/cm^3 and is, to the best of the authors' knowledge, the highest density aqueous phase that has yet been demonstrated. Moreover, in this concentration the interparticle separation can be controlled in three dimensions. In addition, this method has also been shown to be extremely efficient in the purification and size separation of NPs, with an efficiency of >99.9% and 99.5%, respectively. It should be noted that the minimum weight/size of the NPs that is needed for this method to work is likely to be dependent on specifics of individual equipment/instruments rather than a universal property. Provided that the effective density of the solution directly adjacent to the interface is sufficiently large, then there is no obvious reason to expect any fundamental constraints on particle size. The simplicity, versatility, speed and efficiency of this technique allow it to be widely used for NP handling, while the remarkable physical properties of the resulting solutions will find applications as novel advanced materials. Of particular interest would be to determine the thermal conductivities of such solutions as the confinement of the NPs may significantly enhance the conductivity as compared to water.

EXPERIMENTAL SECTION

Equipment Used. UV–vis measurements were performed with a Nanodrop 2000c spectrometer using PMMA cuvettes. An Eppendorf 5424 centrifuge with a FA-45-24-11 rotor with a radius of 8.4 cm was used, capable of holding 24 × 2 mL centrifuge tubes at an angle of 45° with a maximum relative centrifugal force (RCF) of 20 238*g* (14 680 rpm). A Beckmann Coulter DelsaNano C dynamic light scattering machine was used for hydrodynamic particle sizing and zeta potential measurements. A Leo Gemini 1525 FEGSEM scanning electron microscope and a JEOL 2010 transmission electron microscope were used to size the NPs and demonstrate size separation. A Mettler-Toledo SevenGo Duo pro pH/ion/conductivity meter was used for conductivity measurements.

In all cases, ultrapure water with a resistivity of 18.2 MΩ·cm was used. All chemicals were purchased from Sigma-Aldrich UK and used without further purification. Chemicals used were the following: $HAuCl_4 \cdot \approx 3H_2O$ (fw 339.79 (anhydrous), 99.999% trace metal basis); trisodium citrate dihydrate (fw 294.10, ≥99%); 12-mercaptododecanoic acid (MDDA, fw 232.38, 99%); methanol (MeOH, CHROMASOLV, HPLC grade, ≥99.9%); 1,2-dichloroethane (DCE) (ACS reagent, ≥99.0%).

MDDA stabilized 16 nm gold nanoparticles were prepared as described previously.[10] Briefly, 8.6 mg of $HAuCl_4 \cdot 3H_2O$ (5 mg gold) was dissolved in 95 mL of H_2O and brought to 100 °C. Under stirring, 5 mL of 13.6 mM sodium citrate solution was then added to the refluxing mixture. The initially faint-yellow solution gradually turned dark-blue followed by wine-red over a period of 10 min. At this point the NPs were measured to have a hydrodynamic diameter, electrophoretic mobility, and zeta potential of 20 ± 4 nm, -3.60×10^{-4} cm^2/(V s), and −47.0 mV, respectively. The size of the particles was verified to be 16.3 ± 2.4 nm using an SEM and TEM. Once the reaction had gone to completion (typically 15 min), the temperature was reduced to 60 °C. This was followed by the addition of MDDA (5 mg) dissolved in MeOH (0.5 mL). The functionalization was allowed to continue for at least 1 h to ensure complete monolayer coverage, after which the mixture was allowed to slowly cool with continuous stirring for at least an extra hour. The excess MDDA precipitated out and was removed by filtration. The functionalized NP typically had a hydrodynamic diameter of 26 ± 7 nm, electrophoretic mobility of -4.37×10^{-4} cm^2/(V s), and a zeta potential of −57.0 mV. The solution typically had a conductivity of 217 μS/cm.

The 43 nm gold particles were synthesized as above with the exception of adding 5 mL of 6.39 mM sodium citrate solution to the refluxing gold salt solution. These particles were not subsequently functionalized with MDDA. After synthesis, the concentration of the citrate ions in the solution was adjusted to be equivalent to that of the 16 nm solution. The final particles had a hydrodynamic diameter of 64.7 ± 30.5 nm, while SEM showed an average particle size of 43 ± 4 nm.

In all experiments, a 2 mL centrifuge tube, with 0.5 mL of DCE and 1 mL of NP solution, was used. To pellet the 16 nm particles, the maximum RCF setting on the centrifuge of 20 238*g*

for 15 min was applied. In the size-separation experiments, a 1:1 (vol/vol) mixture of 16 and 43 nm particles was used and centrifuged at 1503*g* (a lower RCF was chosen to limit aggregation of the citrate stabilized 43 nm NPs) for 15 min. The pellets were extracted by pipetting out the residual aqueous phase, followed by extraction of the pellet encapsulated in a small amount of DCE which was then allowed to evaporate off.

X-ray experiments were carried out on the high brilliance beamline I22 at Diamond Light Source (DLS), U.K. The synchrotron X-ray beam was tuned to a wavelength of 0.688 Å ($E = 18$ keV), having beam dimensions of approximately 320 × 250 μm, and had a typical flux of 10^{12} photons s^{-1}. The distance between the sample and detector was set at 2.2 m, and the 2-D diffraction patterns were recorded on a Pilatus 2M detector. Silver behenate (a = 58.38 Å) was used to calibrate the low-angle X-ray diffraction data. Diffraction images were analyzed using the IDL-based AXcess software package, developed in-house by Dr A. Heron.[26] The measured X-ray spacings are accurate to ±0.1 Å.

Conflict of Interest: The authors declare no competing financial interest.

Supporting Information Available: Scanning electron micrographs of size separation, technique for density and LSPR measurements and details on FIT simulations. This material is available free of charge *via* the Internet at http://pubs.acs.org.

Acknowledgment. This work was funded in part by an ERC starting investigator grant and EPSRC grants EP/G00465X and EP/H046593/1. The authors would like to thank Professor John Seddon for useful discussions regarding the XRD diffraction experiments and to Christopher Wood for performing the TEMs. AAK and AD would like to thank EU FP7 'Nanodetector' grant (NMP4-SE-2012-280478).

REFERENCES AND NOTES

1. Cecchini, M. P.; Turek, V. A.; Paget, J.; Kornyshev, A. A.; Edel, J. B. Self-Assembled Nanoparticle Arrays for Multiphase Trace Analyte Detection. *Nat. Mater.* **2013**, *12*, 165–171.
2. Cecchini, M. P.; Hong, J.; Lim, C.; Choo, J.; Albrecht, T.; deMello, A. J.; Edel, J. B. Ultrafast Surface Enhanced Resonance Raman Scattering Detection in Droplet-Based Microfluidic Systems. *Anal. Chem.* **2011**, *83*, 3076 3081.
3. Cecchini, M. P.; Stapountzi, M. A.; McComb, D. W.; Albrecht, T.; Edel, J. B. Flow-Based Autocorrelation Studies for the Detection and Investigation of Single-Particle Surface-Enhanced Resonance Raman Spectroscopic Events. *Anal. Chem.* **2011**, *83*, 1418–1424.
4. Wilton-Ely, J. D. E. T. The Surface Functionalisation of Gold Nanoparticles with Metal Complexes. *Dalton Trans.* **2008**, 25–29.
5. Cheong, K. H.; Yi, D. K.; Lee, J.-G.; Park, J.-M.; Kim, M. J.; Edel, J. B.; Ko, C. Gold Nanoparticles for One Step DNA Extraction and Real-Time PCR of Pathogens in a Single Chamber. *Lab Chip* **2008**, *8*, 810–813.
6. Llevot, A.; Astruc, D. Applications of Vectorized Gold Nanoparticles to the Diagnosis and Therapy of Cancer. *Chem. Soc. Rev.* **2012**, *41*, 242–257.
7. Abid, A. D.; Kanematsu, M.; Young, T. M.; Kennedy, I. M. Arsenic Removal from Water Using Flame-Synthesized Iron Oxide Nanoparticles with Variable Oxidation States. *Aerosol Sci. Technol.* **2012**, *47*, 169–176.
8. Garnett, E. C.; Cai, W.; Cha, J. J.; Mahmood, F.; Connor, S. T.; Greyson Christoforo, M.; Cui, Y.; McGehee, M. D.; Brongersma, M. L. Self-Limited Plasmonic Welding of Silver Nanowire junctions. *Nat. Mater.* **2012**, *11*, 241–249.
9. Brown, M. D.; Suteewong, T.; Kumar, R. S. S.; D'Innocenzo, V.; Petrozza, A.; Lee, M. M.; Wiesner, U.; Snaith, H. J. Plasmonic Dye-Sensitized Solar Cells Using Core− Shell Metal− Insulator Nanoparticles. *Nano Lett.* **2011**, *11*, 438.
10. Turek, V. A.; Cecchini, M. P.; Paget, J.; Kucernak, A. R.; Kornyshev, A. A.; Edel, J. B. Plasmonic Ruler at the Liquid−Liquid Interface. *ACS Nano* **2012**, *6*, 7789–7799.
11. Vigderman, L.; Zubarev, E. R. Starfruit-Shaped Gold Nanorods and Nanowires: Synthesis and Sers Characterization. *Langmuir* **2012**, *28*, 9034.
12. Grzelczak, M.; Perez-Juste, J.; Mulvaney, P.; Liz-Marzan, L. M. Shape Control in Gold Nanoparticle Synthesis. *Chem. Soc. Rev.* **2008**, *37*, 1783–1791.
13. Ahammed, S.; Saha, A.; Ranu, B. C. Hydrogenation of Azides over Copper Nanoparticle Surface Using Ammonium Formate in Water. *J. Org. Chem.* **2011**, *76*, 7235–7239.
14. Jana, N. R.; Gearheart, L.; Murphy, C. J. Wet Chemical Synthesis of High Aspect Ratio Cylindrical Gold Nanorods. *J. Phys. Chem. B* **2001**, *105*, 4065–4067.
15. Faulds, K.; Littleford, R. E.; Graham, D.; Dent, G.; Smith, W. E. Comparison of Surface-Enhanced Resonance Raman Scattering from Unaggregated and Aggregated Nanoparticles. *Anal. Chem.* **2003**, *76*, 592–598.
16. Sun, Y.; Xia, Y. Shape-Controlled Synthesis of Gold and Silver Nanoparticles. *Science* **2002**, *298*, 2176–2179.
17. Jin, R.; Charles Cao, Y.; Hao, E.; Metraux, G. S.; Schatz, G. C.; Mirkin, C. A. Controlling Anisotropic Nanoparticle Growth through Plasmon Excitation. *Nature* **2003**, *425*, 487–490.
18. Li, Y.; Zhou, J.; Tung, S.; Schneider, E.; Xi, S. A Review on Development of Nanofluid Preparation and Characterization. *Powder Technol.* **2009**, *196*, 89–101.
19. Bresme, F.; Oettel, M. Nanoparticles at Fluid Interfaces. *J. Phys.: Condens. Matter* **2007**, *19*, 413101.
20. Flatté, M. E.; Kornyshev, A. A.; Urbakh, M. Understanding Voltage-Induced Localization of Nanoparticles at a Liquid−Liquid Interface. *J. Phys.: Condens. Matter* **2008**, *20*, 073102.
21. Liu, X.; Atwater, M.; Wang, J.; Huo, Q. Extinction Coefficient of Gold Nanoparticles with Different Sizes and Different Capping Ligands. *Colloids Surf., B* **2007**, *58*, 3–7.
22. Koroznikova, L.; Klutke, C.; McKnight, S.; Hall, S. The Use of Low-Toxic Heavy Suspensions in Mineral Sands Evaluation and Zircon Fractionation. *J. South. Afr. Inst. Min. Metall.* **2008**, *108*, 25–33.
23. Jana, N. R. Gram-Scale Synthesis of Soluble, near-Monodisperse Gold Nanorods and Other Anisotropic Nanoparticles. *Small* **2005**, *1*, 875–882.
24. Akbulut, O.; Mace, C. R.; Martinez, R. V.; Kumar, A. A.; Nie, Z.; Patton, M. R.; Whitesides, G. M. Separation of Nanoparticles in Aqueous Multiphase Systems through Centrifugation. *Nano Lett.* **2012**, *12*, 4060–4064.
25. Chithrani, B. D.; Ghazani, A. A.; Chan, W. C. W. Determining the Size and Shape Dependence of Gold Nanoparticle Uptake into Mammalian Cells. *Nano Lett.* **2006**, *6*, 662–668.
26. Seddon, J. M.; Squires, A. M.; Conn, C. E.; Ces, O.; Heron, A. J.; Mulet, X.; Shearman, G. C.; Templer, R. H. Pressure-Jump X-Ray Studies of Liquid Crystal Transitions in Lipids. *Philos. Trans. R. Soc., A* **2006**, *364*, 2635–2655.